




4-11-2018

Surface Roughness Dependence of Inkjet Printing of Ag Nanoparticles

Ming Yuan Chuang

Quattrone Nanofabrication Facility, chuangm@seas.upenn.edu

Follow this and additional works at: https://repository.upenn.edu/scn_protocols

 Part of the [Engineering Commons](#), [Life Sciences Commons](#), and the [Physical Sciences and Mathematics Commons](#)

Chuang, Ming Yuan, "Surface Roughness Dependence of Inkjet Printing of Ag Nanoparticles", *Protocols and Reports*. Paper 51.
https://repository.upenn.edu/scn_protocols/51

This paper is posted at ScholarlyCommons. https://repository.upenn.edu/scn_protocols/51
For more information, please contact repository@pobox.upenn.edu.

Surface Roughness Dependence of Inkjet Printing of Ag Nanoparticles

Abstract

This report describes dependence of the inkjet printing on the surface roughness of normal PI film, ultra-smooth PI film, and polished Si wafer. The printing line width and LER are discussed by the line spreading constraint due to the limited volume of the droplet, vaporization of the solvent by the substrate temperature, the contact angle of the ink, and the surface roughness of the substrate. It is also shown that the minimum line width of $\sim 21\mu\text{m}$ is achieved on the Si wafer. Furthermore, the optimization of the substrate temperature for sintering of Ag nanoparticle is discussed.

Keywords

Inkjet printing, Ag nanoparticles, surface roughness


Disciplines

Engineering | Life Sciences | Physical Sciences and Mathematics

Creative Commons License



This work is licensed under a [Creative Commons Attribution-Share Alike 4.0 License](https://creativecommons.org/licenses/by-sa/4.0/).

	Technical Report	Document No:
	(Graduate Student Fellow Program)	Revision:
	Surface Roughness Dependence of Inkjet Printing of Ag Nanoparticles	Author: Ming-Yuan Chuang

1. Introduction

Thermal drop-on-demand (DOD), and piezoelectric DOD inkjet printing technologies have been reported as the successful inkjet drop generation technologies, and have widely been used in printed flexible electronics, display, sensors, bio-arrays, solar cells, and ceramic component manufacture for the last decade.^{1,2,3,4} Especially piezoelectric DOD printing has been chosen for most applications in printing functional materials.⁴ The piezoelectric DOD inkjet printer employs a piezoelectric element to drive current through the nozzles, ejecting droplets on the substrate according to the pre-defined digital design. DOD inkjet printing does not only provide a cost and time effective additive process for mask-less micro-patterning, but also can digitally control the ejection of ink droplets of defined volume and print a pattern precisely at the desired location of the substrate.

The goal of this project is to perform on-site inspection of piezoelectric DOD inkjet printer, Dimatix (DMP-2831, Fujifilm), at Quattrone Nanofabrication Facility (QNF), and to optimize the printing conditions on polyimide (PI) film. In the previous report,⁵ the rheological analysis confirmed that the present Ag nanoparticle ink was suitable for the piezoelectric DOD printing for both of 1 pL and 10 pL cartridges, and the printing parameters were also optimized. On the other hand, it was found that the line edge roughness (LER) was seriously affected by the surface roughness of the substrate. This report describes dependence of the inkjet printing on the surface roughness of normal PI film, ultra-smooth PI film, and polished Si wafer. The printing line width and LER are discussed by the line spreading constraint due to the limited volume of the droplet, vaporization of the solvent by the substrate temperature, the contact angle of the ink, and the surface roughness of the substrate. It is also shown that the minimum line width of ~21 μ m is achieved on the Si wafer. Furthermore, the optimization of the substrate temperature for sintering of Ag nanoparticle is discussed.

2. Experimental Section

A. Materials

127 μ m thick normal PI films were purchased from McMaster-Carr. ~25 μ m thick ultra-smooth PI films were purchased from NeXolve. Prime grade Si wafers with the surface roughness of less than 1 nm were purchased from Wafer World. The 30-35 wt% Ag dispersion in triethylene glycol monomethyl ether was purchased from Sigma Aldrich. The PI films and Si wafers were sonicated in acetone and isopropyl alcohol (IPA) for 5 min each and dried with dry nitrogen gas, before printing. The contact angles of the ink with normal and ultra-smooth PI films and Si wafer were 10.6, 0.0, and 16.3 $^{\circ}$, respectively.

B. Measurement

Optical microscope images were measured using Zeiss Imager-M2m Optical Microscope. The surface roughness and 3D profile of PI film were measured using Zygo New View 7300 optical profiler. Scanning electron microscope (SEM) images were measured using JOEL JSM-7500F. The calculation of line width roughness and line edge roughness is based on the optical microscope images. Figure 1 shows the 14 data sampling from the printed line for (a) line width roughness (LWR) and (b) line edge roughness (LER). The sampling space between the points is 100 μ m.⁶

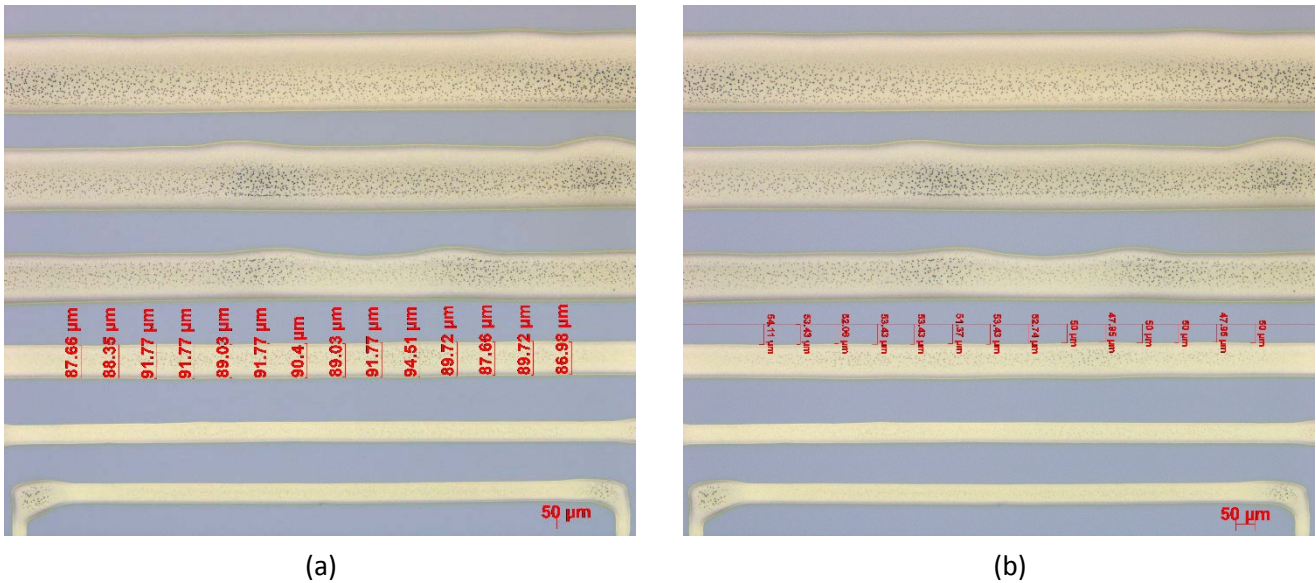


Figure 1. The sampling of (a) LWR and (b) LER data points. The sampling space between the points is 100μm. The substrate is a Si wafer.

C. Cartridge and Printing setup

Table 1 shows printing setups of 1 pL and 10 pL cartridges used in this study. The cartridge temperature and jetting voltage are tuned because of the deviation in jetting performance from nozzle to nozzle. The number of the active nozzles was set up to be one out of sixteen, and the maximum jetting frequency was 5 kHz. The print height was set up to be 0.4 mm. It is reported that increase in the substrate temperature can reduce line width and improve the continuity of printed lines.⁷ Therefore, the substrate temperature used in this report was optimized as high as possible. When the substrate temperature was higher than the optimized one, the ink droplet was dried out even before printing the next droplet, resulting in a line with dots overlapped but not merged. After printing, the ink was sintered at 150 °C for 30 min on a hot plate to remove the organic solvent and fuse Ag nanoparticles together to form conductive tracks. Dependence of aggregation of Ag nanoparticles on the sintering temperature will also be discussed later.

Table 1. Printing setup for 1 pL and 10 pL cartridge.

Substrate	Substrate Temperature	Cartridge Temperature	Jetting Voltage	Drop spacing
1 pL cartridge				
Normal PI film	50 °C	35 °C	20 V	20 μm
Ultra-smooth PI film	50 °C	40 °C	14 V	20 μm
Silicon wafer	45 °C	40 °C	15 V	20 μm
10 pL cartridge				
Normal PI film	50 °C	40 °C	40 V	40 μm
Ultra-smooth PI film	60 °C	40 °C	40 V	40 μm
Silicon wafer	60 °C	40 °C	40 V	30 μm

3. Results and Discussion

3.1. Inkjet printing on normal and ultra-smooth PI films, and Si wafer

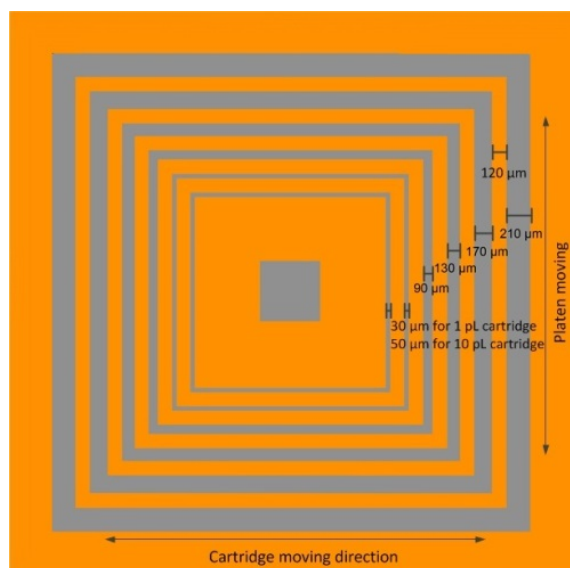


Figure 2. Illustration of the printing pattern.

Figure 2 shows illustration of the printing pattern. Figure 3 shows the 3D surface profiles of (a) normal PI film, (b) ultra-smooth PI film, and (c) Si wafer, which have the root-mean-square (RMS) surface roughnesses of 37.5, 2.1, and 0.9 nm, respectively (the z-scales of the images are not the same). Figure 4 shows optical microscope images of the inkjet printing using 1 pL cartridge on (a) normal PI film, (b) ultra-smooth PI film, and (c) Si wafer, respectively. Figure 5 exhibits optical microscope images of the inkjet printing using 10 pL cartridge on (a) normal PI film, (b) ultra-smooth PI film, and (c) Si wafer, respectively. As seen in figures 4 and 5, the LER of the inkjet printing decreases with decreasing in the surface roughness of the substrate. Especially, the LER of the printing on Si wafer is much smaller than that on PI films, as discussed later.

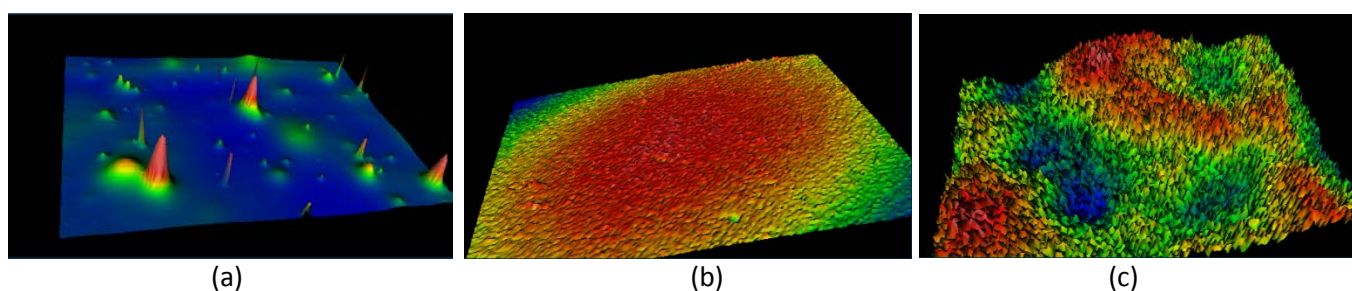


Figure 3. 3D surface profiles of (a) normal PI film, (b) ultra-smooth PI film, and (c) Si wafer, which have the RMS surface roughness of 37.5, 2.1, and 0.9 nm, respectively. The field of view is $140\ \mu\text{m} \times 110\ \mu\text{m}$. The Z-scales of the images are not the same.

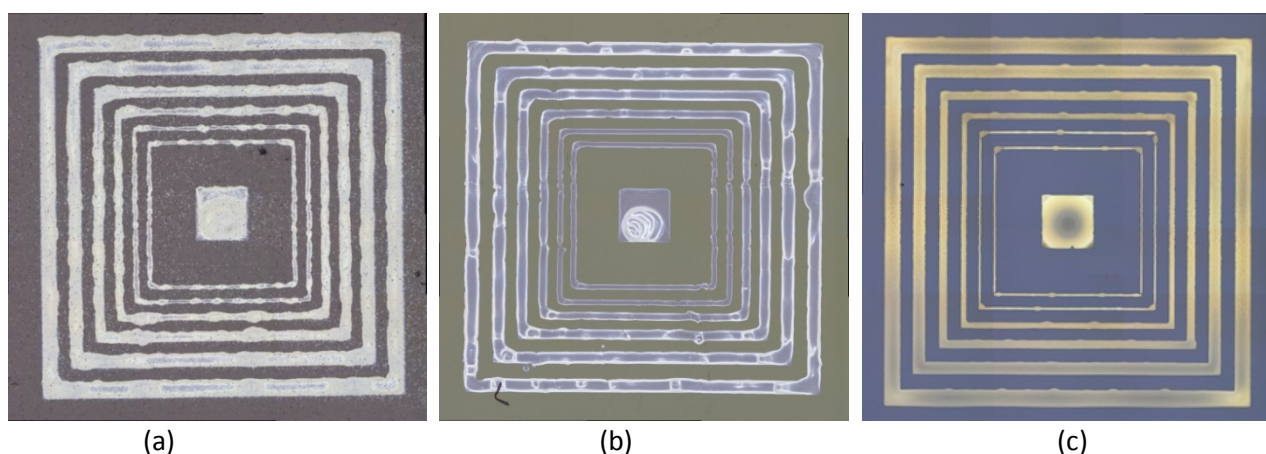


Figure 4. Optical microscope images of the inkjet printing using 1 pL cartridge on (a) a normal PI film, (b) an ultra-smooth PI film, and (c) a Si wafer.

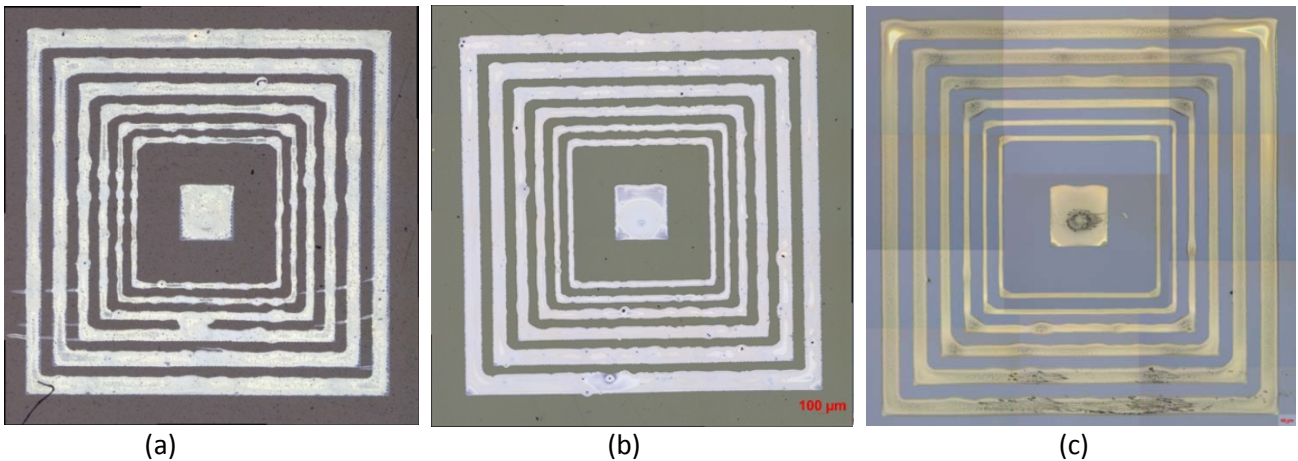


Figure 5. Optical microscope images of the inkjet printing using 10 pL cartridge on (a) a normal PI film, (b) an ultra-smooth PI film, and (c) a Si wafer. The tone change in (c) is due to stitching the images.

Figures 6 and 7 show expanded optical microscope images of the inkjet printing of 30 and 90 μm width vertical and horizontal lines using 1 pL cartridge, respectively. The substrates are (a) normal PI film, (b) ultra-smooth PI film, and (c) Si wafer in figures 6 and 7. Table 2 indicates average line widths (W_{avg}), standard deviations of the LWR (σ_{LWR}), standard deviations of the LER (σ_{LER}) of the Ag nanoparticle lines inkjet printed on normal and ultra-smooth PI films and Si wafer.

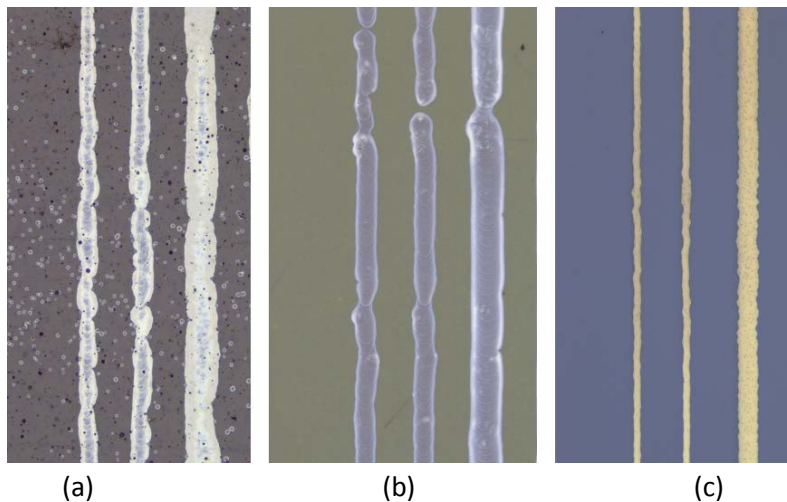


Figure 6. Expanded optical microscope images of the inkjet printing of 30 and 90 μm width vertical lines using 1 pL cartridge. The substrates are (a) normal PI film, (b) ultra-smooth PI film, and (c) Si wafer. The setting widths in each image are 30, 30, and 90 μm from the left to the right side, respectively. The actual widths are shown in Table 2. The contact angles of the ink with the normal PI film, ultra-smooth PI film, and Si wafer were 10.6, 0.0, and 16.3 $^\circ$, respectively.

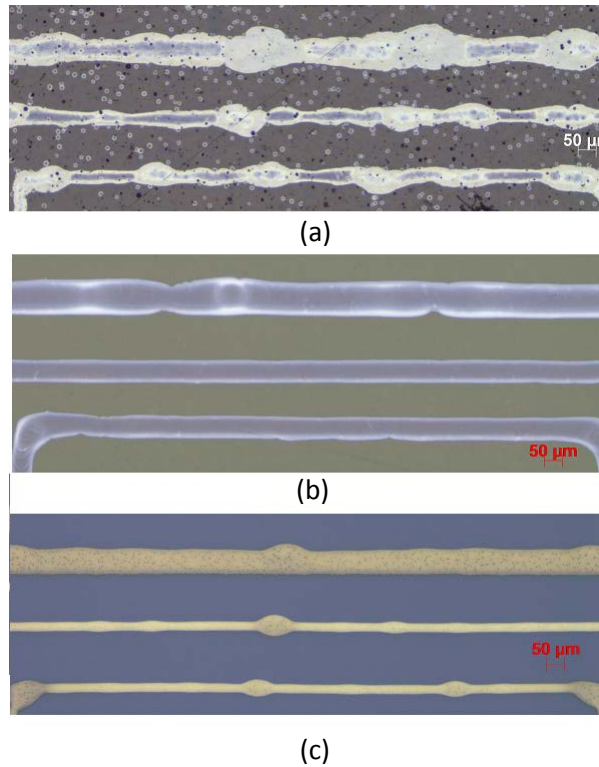


Figure 7. Expanded optical microscope images of the inkjet printing of 30 and 90 μm width horizontal lines using 1 pL cartridge. The substrates are (a) normal PI film, (b) ultra-smooth PI film, and (c) Si wafer. The setting widths in each image are 30, 30, and 90 μm from the bottom to the top side, respectively. The actual widths are shown in Table 2. The contact angles of the ink with the normal PI film, ultra-smooth PI film, and Si wafer were 10.6, 0.0, and 16.3 $^\circ$, respectively.

Table 2. Average line widths (W_{avg}), standard deviations of the LWR (σ_{LWR}), standard deviations of the LER (σ_{LER}) of the Ag nanoparticle lines inkjet printed on normal and ultra-smooth PI films and Si wafer.

	1 pL cartridge						10 pL cartridge					
	Vertical			Horizontal			Vertical			Horizontal		
	V1-1	V1-2	V2	H1-1	H1-2	H2	V1-1	V1-2	V2	H1-1	H1-2	H2
Setting Width	30	30	90	30	30	90	50	50	90	50	50	90
Normal PI film												
W_{avg}	49.6	51.8	92.9	49.8	46.5	87.8	62.4	64.8	91.1	65.0	65.8	93.3
σ_{LWR}	7.7	8.3	9.0	13.2	12.6	20.2	9.6	6.9	14.7	11.9	14.6	11.4
σ_{LER}	5.3	6.3	7.4	6.5	7.1	12.2	6.0	6.1	4.5	8.0	6.4	5.9
Ultra-smooth PI film												
W_{avg}	62.2	63.7	98.4	61.4	62.4	94.7	65.1	66.7	100.7	78.7	77.8	112.6
σ_{LWR}	7.9	7.7	12.0	2.1	1.3	6.7	2.1	2.3	5.0	6.3	6.3	8.9
σ_{LER}	7.4	4.8	8.2	2.9	0.9	5.7	2.6	2.9	6.4	5.8	4.9	6.7
Si wafer												
W_{avg}	21.7	21.5	61.1	27.4	26.8	69.5	42.1	41.7	72.7	52.9	51.8	90.0
σ_{LWR}	1.3	1.1	2.0	5.8	2.5	4.5	1.6	2.2	9.2	1.6	1.3	2.1
σ_{LER}	1.5	1.9	2.2	3.7	2.7	4.6	1.8	2.0	4.5	1.9	1.4	2.1

(in μm)

The limit of inkjet printing line width of 1 pL droplet should be around 12 μm , assuming that the 1 pL droplet is a perfect sphere. The printing line width should increase with increasing in the contact angle of the droplet with the substrate. Actually, Table 2 shows that the average vertical 30 μm line widths on the ultra-smooth PI film, the normal PI film, and the Si wafer are ~ 63 , ~ 50 , and ~ 21 μm , respectively, which correspond to a trend of the contact angles of the ink ~ 0 , 10.6, and 16.3 $^\circ$, respectively. It is also seen that the printing line width is seriously affected by the contact angle of the ink rather than by the surface roughness of the substrate. Although the contact angle of the ink with the ultra-smooth PI film is ~ 0 $^\circ$, the ~ 63 μm printing line width should be ascribed with the ink spreading constraint due to the limited volume of 1 pL and vaporization of the solvent at the substrate temperature of 50 $^\circ\text{C}$. The ~ 50 μm printing line width on the normal PI film is narrower by ~ 13 μm than that on the ultra-smooth PI film, due to the additional effects on the contact angle of 10.6 $^\circ$ and the surface roughness of the substrate. Difference in the printing line width by ~ 42 μm between the ultra-smooth PI film and the Si wafer should arise from the ink spreading constraint due to vaporization of the solvent, and the contact angle of 16.3 $^\circ$, because the surface roughness of the Si substrate is negligible small.

The LER should be independent of the set-up line width because it is attributed with the non-parallel contact line pinning and the bulge instability,^{8,9} which are related to the contact angle, the printing speed, and the surface roughness. Although the data on σ_{LER} in Table 2 is scattered, suggesting that the 14 data sampling is not still enough, the total σ_{LER} for the normal PI film, the ultra-smooth PI film, and the Si wafer can be calculated to be 7.1, 5.4, and 2.7 μm , respectively, and follow the trend of the surface roughness. It should also be pointed out that scratches and dusts on a PI film cause the bulge instability. Especially, dusts easily adsorb on the PI film due to static electricity in a normal environment. Since this study has been carried out in a normal environment, it is likely that the bulges on the line in figures 6 and 7 are caused by some dusts on the PI films.

3.2 Aggregation of Ag nanoparticles depending on sintering temperature

Figure 8 shows SEM images of Ag nanoparticles printed on Si substrate after annealing at (a) 100, (b) 150, and (c) 350 $^\circ\text{C}$ for 30 min. Figure 8(a) clearly shows the boundary among the Ag nanoparticles, revealing that the particles are just in contact with each other at 100 $^\circ\text{C}$. Figure 8(b) shows that the annealing at 150 $^\circ\text{C}$, recommended by the manufacturer, results in an adequate fusion of the Ag nanoparticles. On the other hand, figure 8(c) exhibits that the annealing at 350 $^\circ\text{C}$ is too high for the sintering because 500 to 600 nm diameter fused-aggregation of Ag nanoparticles is formed, disconnecting the network of Ag nanoparticles. This result indicates that the sintering of the Ag nanoparticle ink is highly sensitive to temperature, and that an inadequate control of annealing temperature will strongly affect the performance of conductive ink.

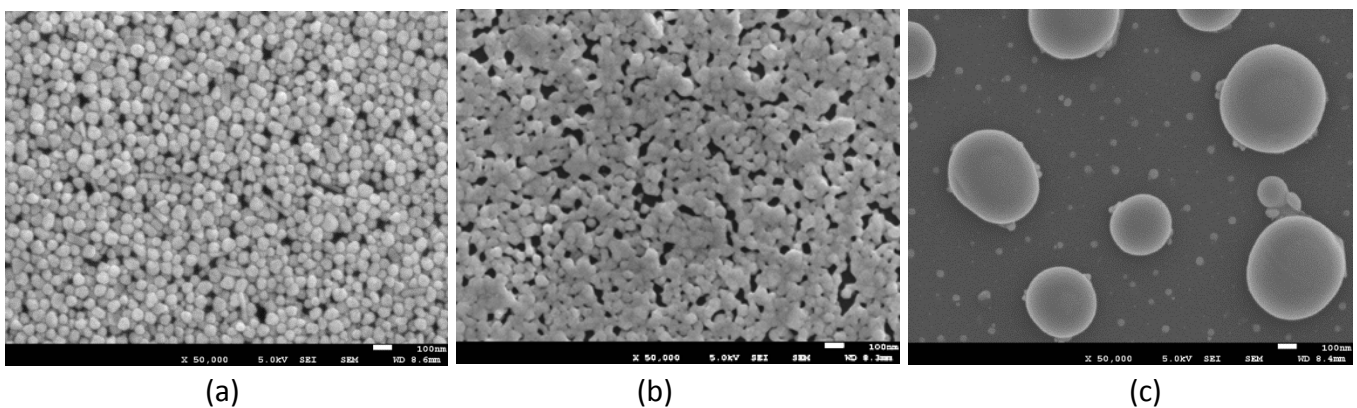


Figure 8. SEM images of silver nanoparticle ink printed on Si substrate sintered at (a) 100 $^\circ\text{C}$ (b) 150 $^\circ\text{C}$ and (c) 350 $^\circ\text{C}$ for 30 minutes.

4. Summary

This study has shown that the inkjet printing line width was determined by the line spreading constraint due to the limited volume of the droplet, vaporization of the solvent by the substrate temperature, the contact angle of the ink, and the surface roughness of the substrate. Especially the printing line width was seriously affected by the contact angle of the ink rather than by the surface roughness of the substrate. It was also indicated that the minimum line width of $\sim 21\mu\text{m}$ was achieved on Si wafer, and was close to the $12\mu\text{m}$ limit of the printing width. On the other hand, the surface roughness of the substrate had the stronger impact on the LER than the contact angle. The LERs for the normal PI film, the ultra-smooth PI film, and the Si wafer indicated to be 7.1, 5.4, and $2.7\mu\text{m}$, respectively, following the trend of the surface roughness. It has also been revealed that the sintering of the Ag nanoparticle ink was highly sensitive to the annealing temperature. When the temperature was too low, the Ag nanoparticles were not fused each other. However, when the temperature was too high, the nanoparticles over-aggregated, and the network of the nanoparticles was disconnected.

References

- ¹ A. Kamyshny and S. Magdassi, "Conductive Nanomaterials for Printed Electronics", *small* **10**, 3515 (2014).
- ² J. Alamán, R. Alicante, J.I. Peña and C. Sánchez-Somolinos, " Inkjet Printing of Functional Materials for Optical and Photonic Applications", *Materials* **9**, 910 (2016).
- ³ B. Derby, "Printing and Prototyping of Tissues and Scaffolds", *SCIENCE* **338**, 921 (2012).
- ⁴ B. Derby, "Inkjet printing ceramics: From drops to solid", *J. Eur. Cera. Soc.* **31**, 2543 (2011).
- ⁵ M. Y. Chuang, "Inkjet Printing of Ag Nanoparticles using Dimatix Inkjet Printer, No.2", https://repository.upenn.edu/scn_protocols/40/.
- ⁶ Changhwan Shin, "Variation-Aware Advanced CMOS Devices and SRAM".
- ⁷ S-H Lee, K-Y Shin, J Y Hwang, K T Kang and H S Kang, "Silver inkjet printing with control of surface energy and substrate temperature", *J. Micromech. Microeng.* **18** (2008) 075014.
- ⁸ M. Singh , H. M. Haverinen , P. Dhagat , G. E. Jabbour , "Inkjet Printing-Process and Its Applications" *Adv. Mater.* **22**, 673 (2010).
- ⁹ B. Derby, "Inkjet printing ceramics: From drops to solid", *J. Eur. Cera. Soc.* **31**, 2543 (2011).